Supporting Information

High-performance and thermostable wire supercapacitors using mesoporous activated graphene deposited on continuous multilayer graphene

TaeGyeong Lim [a], *Ba Trung Ho* [b], *and Ji Won Suk* [a,b,c,*]

[a] School of Mechanical Engineering, Sungkyunkwan University, Suwon, Gyeonggi-do 16419, Republic of Korea

[b] SKKU Advanced Institute of Nanotechnology (SAINT), Sungkyunkwan University, Suwon, Gyeonggi-do 16419, Republic of Korea

[c] Department of Smart Fab. Technology, Sungkyunkwan University, Suwon, Gyeonggi-do 16419, Republic of Korea

[*] Corresponding author. Tel: +82-31-290-7469. E-mail: jwsuk@skku.edu (J. W. Suk)

Keywords: wire supercapacitor; activated graphene; chemical vapor deposition; thermal stability; current collector

XPS Analysis

The X-ray photoelectron spectroscopy (XPS) C 1s spectra were analyzed using peak deconvolution. The sp^2-hybridized carbon (C=C) bonding located at the binding energy of 284.6 eV was fitted using the asymmetric Doniach–Sunjic line shape.[1, 2] Other spectral components corresponding to the sp^3-hybridized carbon (C–C), C–O, C=O, O=C–O, and π-π* transition were located at 285.6, 286.4, 287.8, 288.9, and 290.8 eV with the Gaussian–Lorentzian product formula, respectively.[3-5] Minimal K 2p peaks appeared at approximately 292–296 eV due to potassium residue left in the activated graphene (AG) after KOH activation.[6]

Electrochemical testing of the synthesized AG

The synthesized AG particles were assembled into electrodes by mixing with 5 wt% polytetrafluoroethylene (PTFE, 60 wt% dispersion in water, Sigma Aldrich) binder. The AG/PTFE mixture was homogenized in an agate mortar and rolled into a 50 μm thick sheet. The electrodes were formed by punching the sheet into 10 mm diameter discs. The supercapacitor test cell was assembled with two identical AG electrodes, two current collectors (conductive polymer film, 2267p, z-flo), a porous separator (3501, Celgard), and a 6 M KOH aqueous electrolyte. The cell assembly was fastened between two stainless steel plates for electrochemical testing.[7]

The CV curves have a rectangular shape within a voltage window of 0–1 V at scan rates of 0.05–0.5 V s^{-1} (**Figure S5a**). The GCD measurements exhibit a linear discharge curve at current densities of 1, 2, 4, and 8 A g^{-1} (**Figure S5b**). A Nyquist plot at frequencies ranging from 50

kHz to 0.1 Hz displays a vertical slope at low frequency, implying a nearly ideal capacitive behavior (**Figure S5c**).[6, 8] The inset of **Figure S5c** shows the equivalent circuit used to fit the Nyquist plot for all supercapacitors tested in this work. The equivalent circuit includes an equivalent resistance (R_s), a double-layer capacitance (C_{DL}), a charge transfer resistance (R_{ct}), and a Warburg element (W_0). Furthermore, the capacitive behavior of the AG electrode is confirmed by the phase angle being close to -90 ° at low frequencies (**Figure S5d**).[9]

The specific gravimetric capacitance of a single electrode was estimated from the GCD curves according to the following equation:

$$C_m = \frac{2I}{m\, dV/dt}$$

where I (A) is the applied constant current, dV/dt (V s^{-1}) is calculated from the slope of the linearly fitted discharge curve over the range of 0.8–0.4 V, and m is the mass of a single electrode. The synthesized AG shows a high gravimetric capacitance of 198 F g^{-1} at a current density of 1 A g^{-1}.

Calculation of electrochemical performance of the wire supercapacitors

The specific areal capacitance of a single electrode was calculated from the CV curves using the following equation:

$$C_A = \frac{2\int I(V)dV}{Av\Delta V}$$

where I (A) is the current in the CV curves, V (V) is the applied voltage, v (V s^{-1}) is the scan rate, ΔV (V) is the total scanning voltage, and A is the area of a single electrode, which

is equal to the circumference of the wire electrode multiplied by the length of the overlapped portion of the two electrodes.

GCD curves were also used to estimate the specific areal capacitance of a single electrode according to the following equation:

$$C_A = \frac{2I}{A\, dV/dt}$$

where I (A) is the applied constant current, dV/dt (V s^{-1}) is calculated from the slope of the linearly fitted discharge curve over the range of 0.8–0.4 V, and A is the area of a single electrode.

The areal energy density (E_A) and power density (P_A) of the device were estimated from the GCD curve using the following formula:

$$E_A = \frac{1}{8} C_A U^2$$

$$P_A = \frac{E_A}{\Delta t_{discharge}}$$

where C_A is the specific areal capacitance of a single electrode, U is the operating voltage window of the device, and $\Delta t_{discharge}$ is the discharge time.

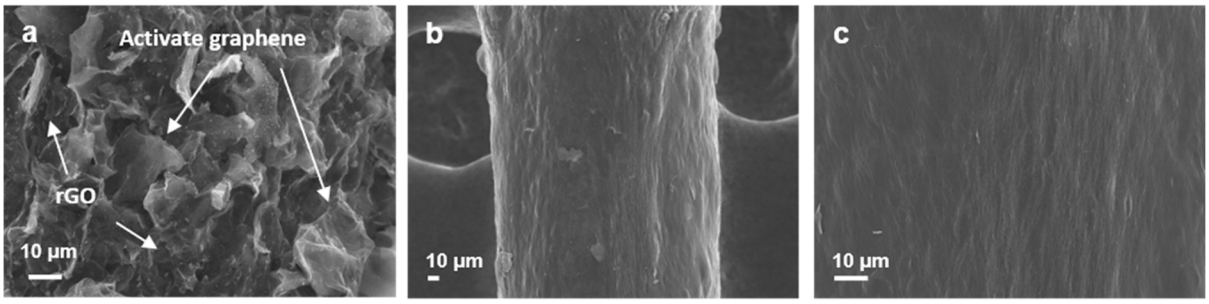

Figure S1. SEM images of the surfaces of (a) AG/rGO@G-Cu and (b, c) rGO@G-Cu wires.

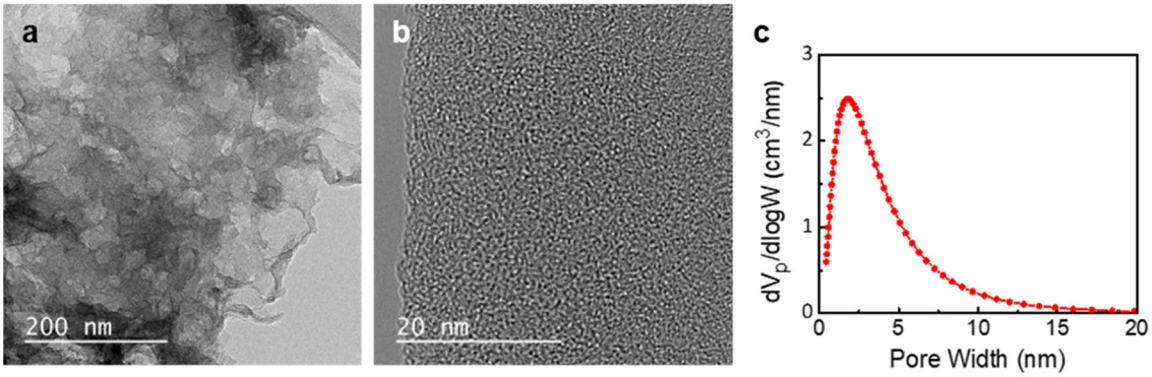

Figure S2. Characterizations of AG. (a, b) HR-TEM images at (a) low and (b) high magnification. (c) Pore size distribution calculated using the NLDFT model.

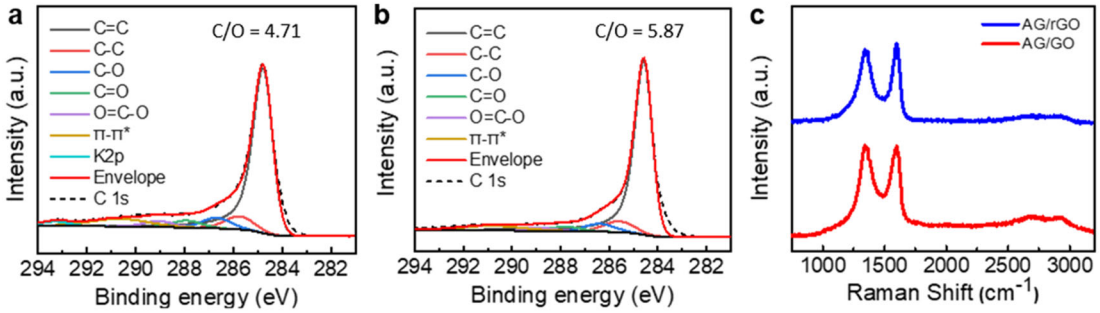

Figure S3. (a, b) XPS C 1s spectra of (a) AG and (b) AG/rGO electrode materials. (c) Raman spectra of AG/GO and AG/rGO.

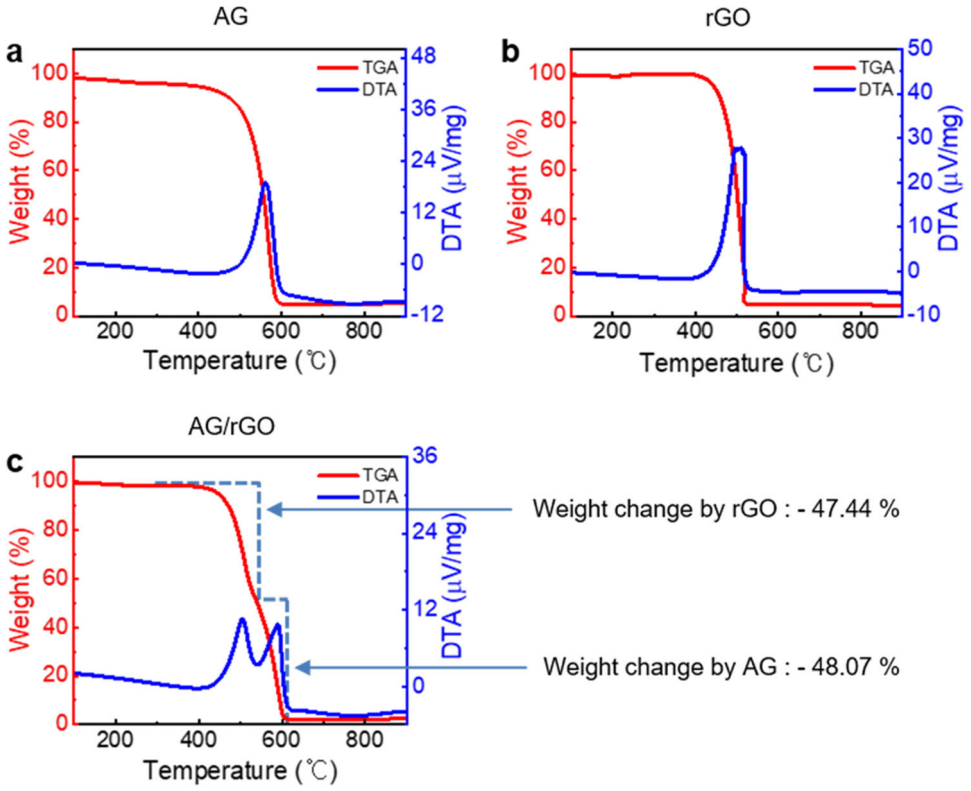

Figure S4. TGA and DTA curves of (a) AG, (b) rGO, and (c) AG/rGO at a temperature range of 20–900 ℃ in air.

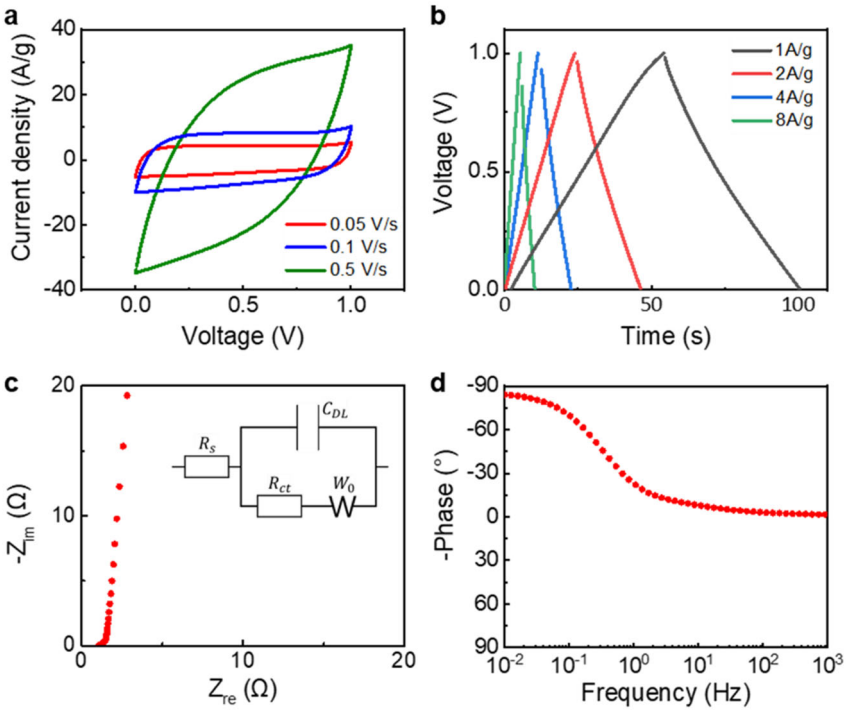

Figure S5. Electrochemical tests of the synthesized AG using a two-electrode supercapacitor with a 6 M KOH electrolyte. (a) CV curves at scan rates ranging from 50 to 500 mV s^{-1}. (b) GCD curves at current densities ranging from 1 to 8 A g^{-1}. (c) Nyquist plot with the equivalent circuit and (d) Bode phase angle plot at frequencies ranging from 50 kHz to 0.1 Hz.

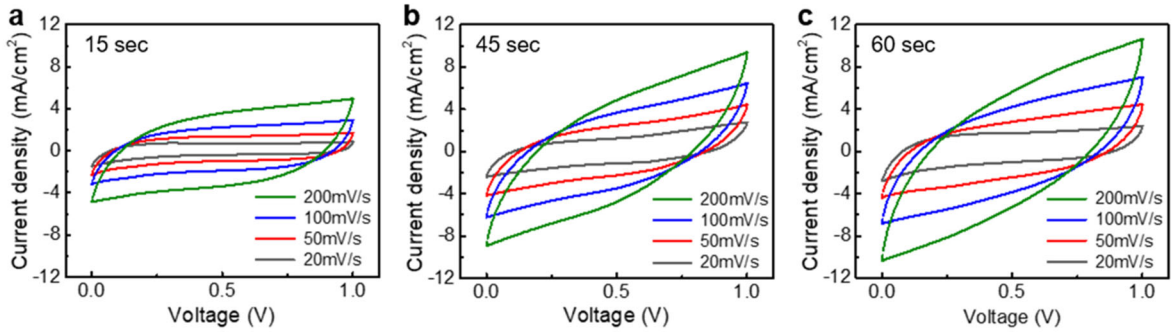

Figure S6. CV curves of the AG/rGO@G-Cu wire supercapacitors at scan rates ranging from 20 to 200 mV s^{-1}. The AG/GO materials were deposited using the EPD process at an applied voltage of 10 V and various deposition times of (a) 15, (b) 45, and (c) 60 s.

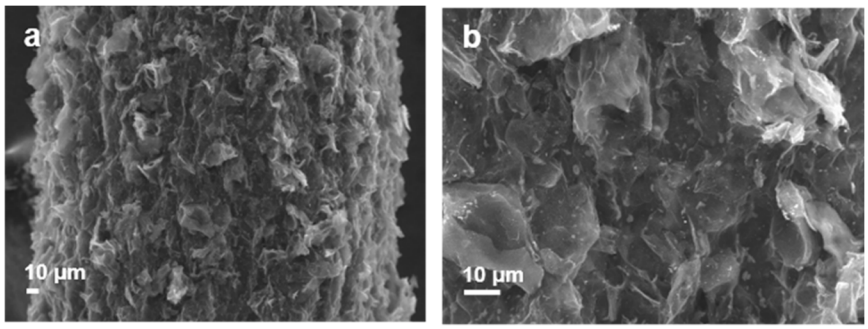

Figure S7. SEM images of the surface of the AG/rGO@G-Cu wire at (a) low and (b) high magnification. The EPD process was performed at an applied voltage of 10 V and a deposition time of 60 s.

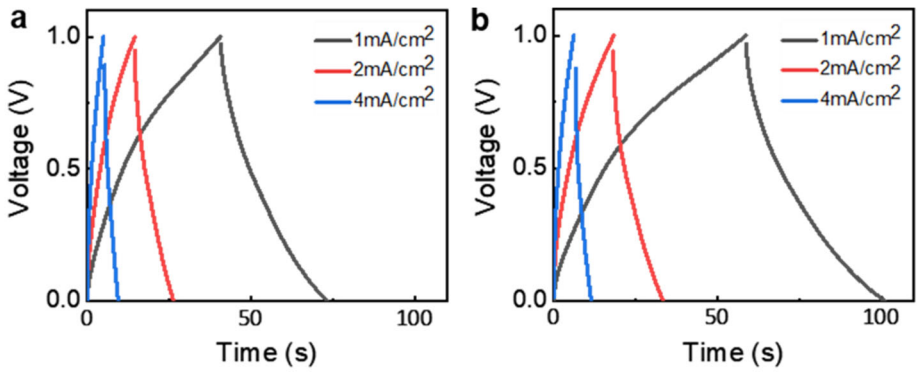

Figure S8. GCD curves of the AG/rGO@G-Cu wire supercapacitor at different current densities. EPD process performed for (a) 30 and (b) 60 s.

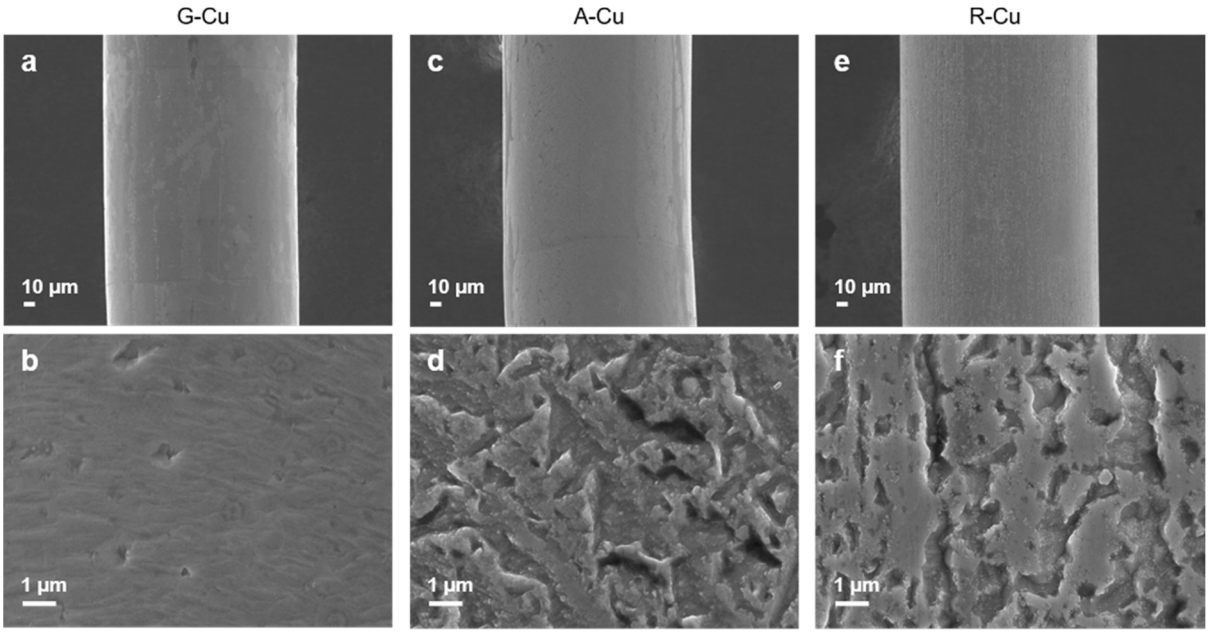

Figure S9. The surface morphology of various Cu wires after each wire was immersed in a gel electrolyte at 80 °C for 1 h. SEM images of (a, b) G-Cu, (c, d) A-Cu, and (e, f) R-Cu wires.

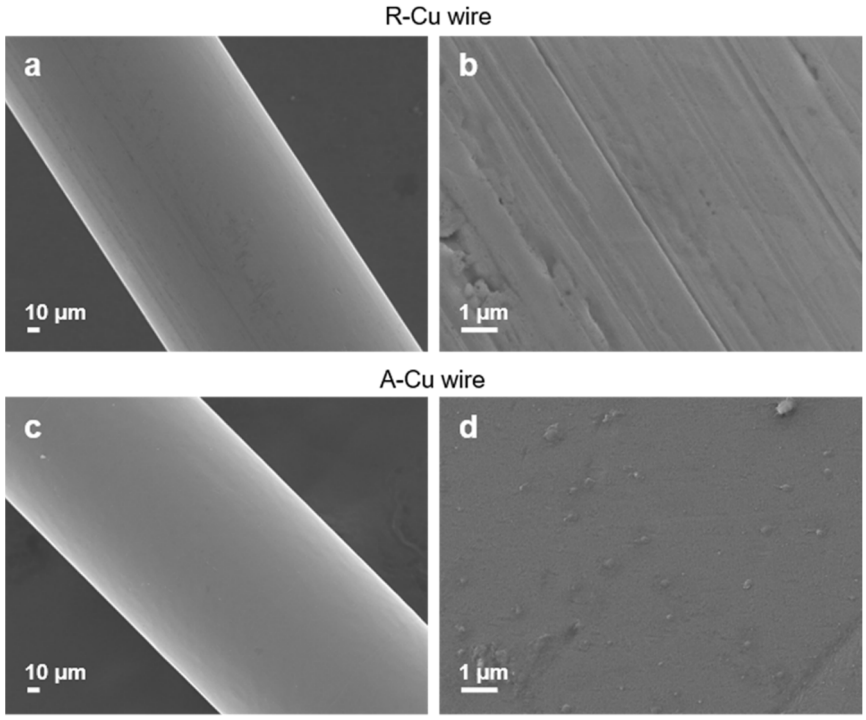

Figure S10. SEM images of (a, b) R-Cu and (c, d) A-Cu wires at low and high magnification.

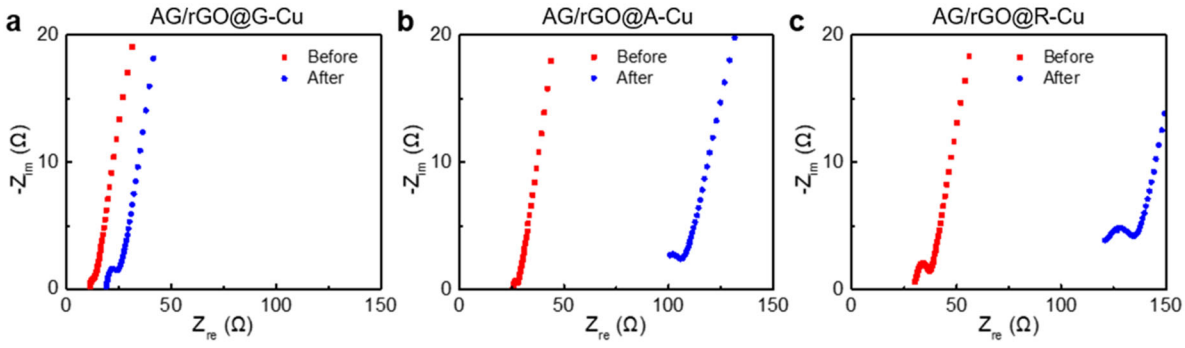

Figure S11. Nyquist plots of the AG/rGO-based wire supercapacitors using (a) G-Cu, (b) A-Cu, and (c) R-Cu at 20 °C before and after the thermal tests.

Table S1. Comparison of electrochemical performance of wire supercapacitors.

Electrode materials	C_A [mF cm^{-2}]	Energy density [μWh cm^{-2}]	Power density [mW cm^{-2}]	ESR [Ω]	Electrolyte	Ref.
AG/rGO@CVD-graphene	130.3 (EPD 60 s)	4.54 (at 1 mA cm^{-2})	0.39 (at 1 mA cm^{-2})	-	PVA/H_3PO_4	This work
		3.42 (at 2 mA cm^{-2})	0.81 (at 2 mA cm^{-2})			
		1.86 (at 4 mA cm^{-2})	1.39 (at 4 mA cm^{-2})			
	104.3 (EPD 30 s)	3.67 (at 1 mA cm^{-2})	0.41 (at 1 mA cm^{-2})	8.0		
		2.86 (at 2 mA cm^{-2})	0.87 (at 2 mA cm^{-2})			
		1.86 (at 4 mA cm^{-2})	1.61 (at 4 mA cm^{-2})			
rGO/CNT core-sheath fiber	177	3.84	0.02	0.55k	PVA/H_3PO_4	[10]
3D graphene-CNT	89.4	-	-	-	PVA/H_2SO_4	[11]
GF@3D-G	1.7	0.17	0.1	-	PVA/H_3PO_4	[12]
Coiled CNT/MnO_2/nylon fiber	40.9	2.6	0.0669	-	PVA/LiCl	[13]
rGO fiber	-	1.68	-	-	PVA/H_3PO_4	[14]

Mesoporous carbon/CNT fiber	39.7	1.77	0.043	-	PVA/H_3PO_4	[15]
GO/rGO fiber	14.3	-	-	-	PVA/H_2SO_4	[16]
Plasma-treated graphene fiber	36.25	0.80	0.02	-	PVA/H_2SO_4	[17]
PPY/CNTs/urethane fiber	-	6.13	0.133	-	PVA/H_3PO_4	[18]
Hollow graphene/conducting polymer	304.5	6.8	0.0166	306.8	PVA/H_3PO_4	[19]

References

1. J. W. Suk, S. Murali, J. An and R. S. Ruoff, *Carbon*, 2012, **50**, 2220-2225.
2. J. W. Suk, W. H. Lee, J. Lee, H. Chou, R. D. Piner, Y. Hao, D. Akinwande and R. S. Ruoff, *Nano Lett.*, 2013, **13**, 1462-1467.
3. D. Yang, A. Velamakanni, G. Bozoklu, S. Park, M. Stoller, R. D. Piner, S. Stankovich, I. Jung, D. A. Field and C. A. Ventrice Jr, *Carbon*, 2009, **47**, 145-152.
4. B. Tang, L. Zhang, R. Li, J. Wu, M. N. Hedhili and P. Wang, *Nanoscale*, 2016, **8**, 1108-1116.
5. J. Kang, T. Lim, M. H. Jeong and J. W. Suk, *Nanomaterials*, 2019, **9**, 815.
6. Y. Zhu, S. Murali, M. D. Stoller, K. Ganesh, W. Cai, P. J. Ferreira, A. Pirkle, R. M. Wallace, K. A. Cychosz and M. Thommes, *science*, 2011, **332**, 1537-1541.
7. M. D. Stoller, S. Park, Y. Zhu, J. An and R. S. Ruoff, *Nano Lett.*, 2008, **8**, 3498-3502.
8. C. Zhang, C. Lei, C. Cen, S. Tang, M. Deng, Y. Li and Y. Du, *Electrochim. Acta*, 2018, **260**, 814-822.
9. T. Kim, G. Jung, S. Yoo, K. S. Suh and R. S. Ruoff, *ACS nano*, 2013, **7**, 6899-6905.
10. L. Kou, T. Huang, B. Zheng, Y. Han, X. Zhao, K. Gopalsamy, H. Sun and C. Gao, *Nat. Commun.*, 2014, **5**, 1-10.
11. Y. Xue, Y. Ding, J. Niu, Z. Xia, A. Roy, H. Chen, J. Qu, Z. L. Wang and L. Dai, *Sci. Adv.*, 2015, **1**, e1400198.
12. Y. Meng, Y. Zhao, C. Hu, H. Cheng, Y. Hu, Z. Zhang, G. Shi and L. Qu, *Adv. Mater.*, 2013, **25**, 2326-2331.
13. C. Choi, S. H. Kim, H. J. Sim, J. A. Lee, A. Y. Choi, Y. T. Kim, X. Lepró, G. M. Spinks, R. H. Baughman and S. J. Kim, *Sci. Rep.*, 2015, **5**, 1-6.
14. G. K. Veerasubramani, K. Krishnamoorthy, P. Pazhamalai and S. J. Kim, *Carbon*, 2016, **105**, 638-648.
15. J. Ren, W. Bai, G. Guan, Y. Zhang and H. Peng, *Adv. Mater.*, 2013, **25**, 5965-5970.
16. Y. Liang, Z. Wang, J. Huang, H. Cheng, F. Zhao, Y. Hu, L. Jiang and L. Qu, *J. Mater. Chem. A*, 2015, **3**, 2547-2551.
17. J. Meng, W. Nie, K. Zhang, F. Xu, X. Ding, S. Wang and Y. Qiu, *ACS Appl. Mater. Interfaces*, 2018, **10**, 13652-13659.
18. J. Sun, Y. Huang, C. Fu, Z. Wang, Y. Huang, M. Zhu, C. Zhi and H. Hu, *Nano Energy*, 2016, **27**, 230-237.
19. G. Qu, J. Cheng, X. Li, D. Yuan, P. Chen, X. Chen, B. Wang and H. Peng, *Adv. Mater.*, 2016, **28**, 3646-3652.